Available online at www.sciencedirect.com
SCIENCE DIRECT®
Journal of Chromatography A, 1006 (2003) 149–170
JOURNAL OF CHROMATOGRAPHY A
www.elsevier.com/locate/chroma

# Converging flow chromatography in constant-pressure mode

Wolfgang Pfeiffer*
*Servico Technico, Ernst-Thaelmann-Strasse 12, D-19322 Wittenberge, Germany*

**Abstract**

Dispersion in chromatographic processes can be reduced to a minimum using converging columns and a curved frit at the outlet. Working at constant pressure at the inlet the internal packing is increasingly compressed by the accelerated flow. Thus the packed bed is stabilized. Under these conditions the observed flux at the outlet and the power input of the pump are inversely related to the viscosity of the eluting solute. Comparing converging flow chromatography (CFC) with classical axial flow chromatography (AFC) and radial flow chromatography (RFC) the stationary phase is used more efficiently in CFC.


*Keywords:* Converging flow chromatography; Radial flow chromatography; Axial flow chromatography; Instrumentation; Column geometry; Pressure control

## 1. Introduction

The shape of the column and its frits at the inlet and the outlet determines the flow profile inside the chromatographic column. They influence the inner packing and consequently also the inner flow in a yet not completely understood but well-defined manner. This interfering influence is called wall effect.

In conventional chromatography a cylindrical column has a flat porous plate at the inlet and outlet. It is perfused by an axial flow. According to the flow direction in its confinement, classical chromatography was called by Rhee et al. about 40 years ago axial flow chromatography (AFC) [1].

This chromatography had evolved 100 years ago. On March 21, 1903 at a Meeting of the Warsaw Society of Natural Scientists, Mikhail Semenovich Tswett presented a lecture entitled ‘‘On a New Category of Adsorption Phenomena and its Application in Biochemical Analysis’’ [2].

When such packed columns are perfused the eluting peaks are slightly skewed. This phenomenon was first traced back in 1969 by Knox [3] to a curvature of the elution front of the separated solutes.

But an axial flow is also possible when one uses not a usual tube but two concentric tubes, which is an annular cylinder. A set of such concentric cylinders have been used by Sada et al. in 1982 to improve the separation using soft packing [4]. In 1994 Yun and Guiochon [5] and Peruth [6] used the annular cylinder model to describe the observed derivations from plug flow more approximate. Both types of cylinder arrangement allow an axial flow.

The annular cylinder is the general mathematical notation that includes both shapes that allow a flow parallel to the symmetry axis ($h$) in AFC (Fig. 1).

The volume of the central cylinder is described as:

$$V = \pi X^2 h \quad (1)$$

*Corresponding author. Tel.: +49-3877-405-360; fax: +49-3877-405-361.
*E-mail address:* servico_technico@web.de (W. Pfeiffer).

0021-9673/03/$ – see front matter 
doi:10.1016/S0021-9673(03)00780-5

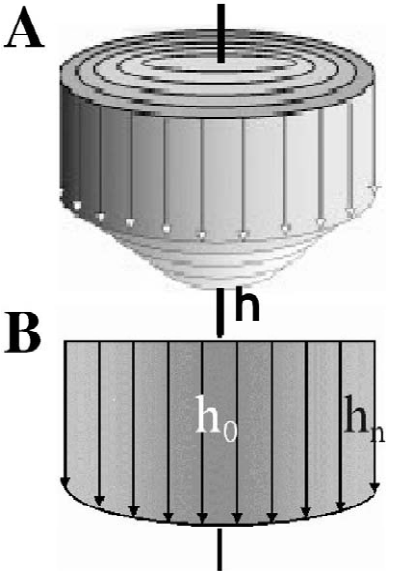


Fig. 1. Axial flow chromatography (AFC). The main flow is parallel to the symmetry axis of the packing, which is axial in an annular cylinder. (A) View on a matrix perfused axially ($h$) in a cylinder (B) cross section through the matrix along $h$ showing different flow-rates due to wall effects.

$X$: radial co-ordinate = constant; $h$: axial coordinate = variable.

The unit-volume element described by Eq. (1) is still generally used in classical chromatography to describe plug flow despite it being well known that the practical obtained elution profiles look different. They cannot be described with one simple volume element only. They are much better described by the annuli model [5,6]:

$$V_0 = \pi X^2 h_0 + \quad (2)$$

$$V_1 = \pi(X_1^2 - X_0^2)h_1 + \quad (3)$$

$$V_2 = \pi\,(X_2^2 - X_1^2)h_2 + \ \ldots V = \pi\,(X_j^2 - X_{j-1}^2)\,h_j \quad (4)$$

The annular cylinder we used as unit-volume for AFC (Compare also section A1 in the Appendix).

The elution profiles of AFC have in most cases the shape of a parabolic cap (concave frit) [7,8]. But also other shapes were observed [9]. We have introduced a method to minimize such distortions of the elution front by a frit at the outlet of the column that is bent in the same way as the elution front. Therewith the adverse effects of internal dispersion on separation can be minimized [10].

Rhee et al. [1] showed theoretically that the geometrical property of the housing determines the flow pattern of the corresponding chromatography. He stated that the separation results from the different column geometries can be directly compared after the correct mathematical transformations (integration respectively coordinate transformations) have been made. The chromatographies in other geometries are shown in Figs. 2 and 3. For the formulation of corresponding unit-volumes compare Appendix A.1.

In 1979 Said calculated the theoretical efficiency of a conical column and came to the conclusion that such a column can be expected to be more efficient than two cylindrical columns with the same total volume but different cross sections [11,12].

In 1988 a Russian group claimed the invention of a conical column. They used a separation funnel filled with glass wool at the outlet as column [13].

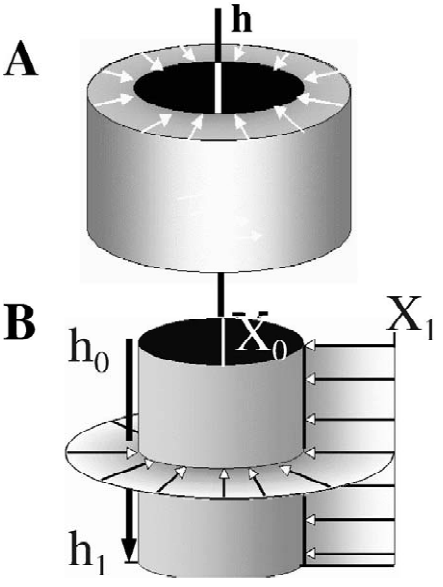


Fig. 2. Radial flow chromatography (RFC). The main flow is perpendicular to the symmetry axis of the packing, which is a radial flow in an (annular) cylinder. (A) View on a matrix perfused in double cylinder radially ($X_1 - X_0$) perpendicular to the symmetry axis $h$ of the height ($h_1 - h_0$). (B) Section through the matrix along $h$ and along ($X_1 - X_0$) showing the convergent flow in direction to the symmetry axis $h$ of the double-cylinder.

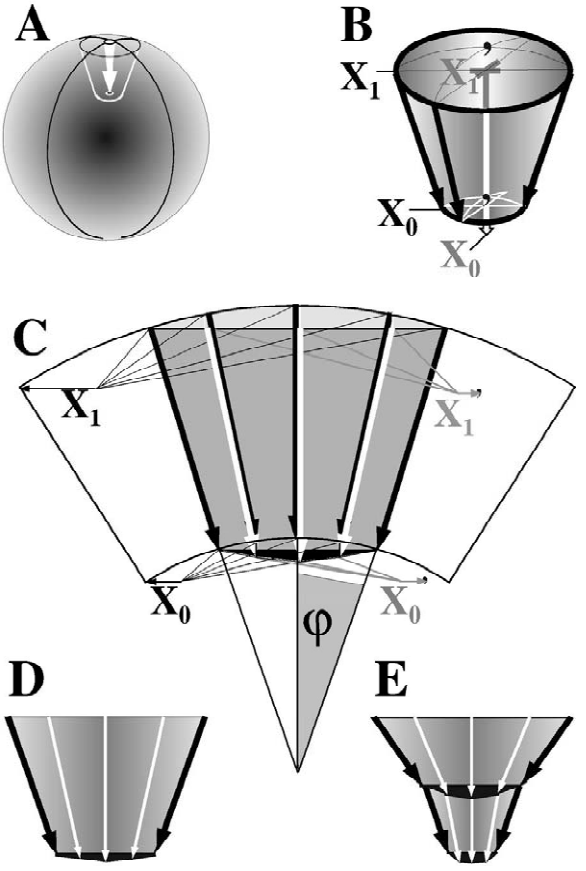


Fig. 3. Converging flow chromatography (CFC). The flow is converging here to the symmetry center of the packing, which is a radial flow in the section ($\varphi$) of an (annular/double) sphere. This flow in the unit element of the double sphere (cone) has an additional symmetry axis ($h$), which corresponds to that of the cylinder. (A) View on a matrix from the outside packed between two concentric spheres and perfused in a central direction. The conical matrix section of interest is highlighted. (B) View on the cone cut from the double sphere with its spherical coordinates $X_0$ and $X_1$. Slightly different from these coordinates are the conical coordinates $X_0'$ and $X_1'$, which show a gray shading. Their black hypes are positioned on the crossing {black ($X_1$) respectively white ($X_0$)} arches of the spherical coordinates. (C) The section through the matrix along the central ($X_1 - X_0$) symmetry axis to the center of the double sphere showing the half-opening angle $\varphi$ of the section of the double-sphere (respectively the half-opening angle of the cone). The black arrows indicate the converging flow in the double-spheres. The white arrows of identical length mark the corresponding flow inside the cone with the compensation of matrix for different migration distances at the outlet. This compensating matrix is shown in black. (D) Cross-section through the cone along this symmetry axis with correction/compensation (in black) at the outlet. (E) Stacking of different corrected cones with different opening angles on each other results in containment with a continuous wall curvature.

About 10 years ago Proseks group started to investigate the efficiency of conical HPLC columns (dimensions of the column 150×4×2.5 mm) and claimed that ''conical columns show a lower flow resistance and less dispersion as conventional columns. The column enables a quicker separation, better reproducibility and up to 50% better peak capacity'' [14]. This work was followed up by the same group [15–18].

At about the same time we investigated the relationship between column geometries and the shape of elution profiles [19–22]. Without knowing from each other we both worked with conical columns, but we used columns of different sizes and variable curvatures $\varphi$, whereas they used only the mentioned small conical column with constant curvature and in addition trapezoidal thin-layer plates. They described both chromatographies together [18]. The trapezoidal thin-layers have to be classified as a radial flow chromatography (RFC) system, which show a small height (=thickness of the layer) and a trapezoidal long lane. It represents a small section from a double cylinder—but not a conical column. It corresponds in its basic geometry to a sector of circular thin-layer separation. Circular thin-layer chromatography with a diverging flow was first described in 1938 by Izmailov [23]. True conical thin-layers came much later. They used diverging flows [24].

Applying the inductive method suggested by Rhee et al. and applied by Gu et al. [25,26] to derive the chromatographic parameters for RFC we have extended their theoretical work to converging flow chromatography (CFC) (compare Sections A.1 and A.2 of the Appendix).

We developed various methodical solutions for the compensation of the observed dispersion. The initial work was done at low pressure with packed beds of soft spheres with volumes between 70 and 1000 ml. In order to achieve a high sample throughput we increased the packing volume to 4 l and ran the column automatically controlled by the inlet pressure in a cyclic manner. Because of the unusual stable fillings we became aware of the fact that a cone is an intrinsic compression column [21]. For the constant pressure mode we developed a very simple column head, which allowed the uncoupling of sample loading and separation. The new head acts the same

time as a pressure sensor with built in pressure feed back control and as a peak sharpening device.

In the constant pressure mode the flux and the power input by the external pump is inversely proportional to the viscosity of the solution passing the outlet. Therefore the specific viscosity of solutes, which are separated can be recorded in CFC online and used for process control.

We calculated the flow parameters for soft sphere packings of CFC at constant inlet pressure of 300 kPa and used the value of the particle Reynolds number to characterize the flow regime. The flow was compared to classical AFC with hard particle packing very slow. But as far we can tell it is still a Darcy's flow, which is inversely dependent on the viscosity. For such slow flows the literature is very sparse and there is no general agreement how far down Darcy's law is valid (see [27]).

## 2. Results

Initially we used packed beds as filter as well as a chromatographic column [19] with the aim of merging two steps of production (filtration and chromatography) into one process step. We chose shapes similar to Buchner funnels, in which we positioned frits at both ends of the cone in the cylindrical sections. The lower fixed frit was holding back the matrix in the cone and the upper frit was laying in the upper cylindrical section on top of the matrix. A thick glass fiber filter was put on top of the frit to ''seal'' the cylindrical sides. This way the upper frit could freely follow volume changes of the matrix. We chose this conical configuration because we could profit from the large surface whilst also undertaking further processing of solutes on the matrix packed into the cone.

The first result was a matrix-bound fractional precipitation. This was achieved by using a soft matrix for size-exclusion chromatography (SEC).

In the SEC matrix the crystals formed in the interstices between the beads because the solutes are too big to penetrate into the beads. The matrix itself however can never become, in this way, completely blocked because the soft spheres are in direct contact with each other and form a network, which allows a slow solute exchange. When the concentration of the buffer solution is changed externally, this change reaches the blocked regions slowly by perfusion through the interconnected network of beads. The crystal surfaces in the blocked interstices become in this way superficially soluble where they face the interconnected beads. In consequence the crystals slide down the interstices until they reach their former size by crystallization and get stuck again. The whole process can now start from the beginning. In consequence a mixture of solutes becomes separated into individual crystal suspensions, which migrate down through the interstices between the porous beads they cannot enter and elute in separate fractions. We have here a chromatographic concentration step combined with a separation. We are not aware of any other chromatographic procedure one can concentrate with. Although the method is slow it is very efficient provided that constant pressure is maintained at the inlet—and the operator stays patient. The advantage of this procedure is that the fractionation of the crystals can be controlled by the buffer gradient from outside. The gradient is independent of the length of column, which is in all the other corresponding methods not the case [28–32]. This chromatographic crystallization method has the advantage that it is generally applicable to all solutes. In theory this method should make substances susceptible to crystallization, which are normally hard to crystallize. We have used this method to crystallize serum proteins.

We want to mention this method here because it demonstrates the potential of convergent flow at constant pressure and its suitability for very ''difficult'' separations of concentrated, viscous or dense solutions. With the versatility of the described method such problems should be overcome.

Initially our work was concentrated on preparative aspects of biochromatography. We focused on the homogeneous perfusion of stable packings of soft spheres to achieve a high efficiency of separation. We desalted precipitated serum and plasma samples by using a column with a packing of 4 l in a cyclic operation. We soon came to the point where we had to compensate for the distortion of the elution front. The distortion was exaggerated by the converging shape of the column and the different migration distance in a cone with a big opening angle. We investigated the influence of differentially shaped

converging columns on the shape of the elution front. These different shapes were analyzed by the peak sharpness (Fig. 4).

The columns were filled with medium-sized Sephadex G-25 beads. A relative low pressure resulted in slow flow-rates. Under the conditions employed the color was strongly retarded. Because of the long retardation times and a careful application of the sample on the open column with a closed outlet one could be sure that the shape dependent dispersion became undisturbed reflected in the elution profiles. The column that resembled a slim wine bottle in its shape resulted in the sharpest peak (A). These columns were made actually from two open cylindrical glass tubes joined together by a glass blower.

Next we used this optimal shape and checked with it the influence of different outwardly curved frits at the outlet on the peak shape (Fig. 5).

Brass plates were manually chased and perforated. They were covered by a glass fiber filter and inserted in the column using an adapter from Bio-Rad with a

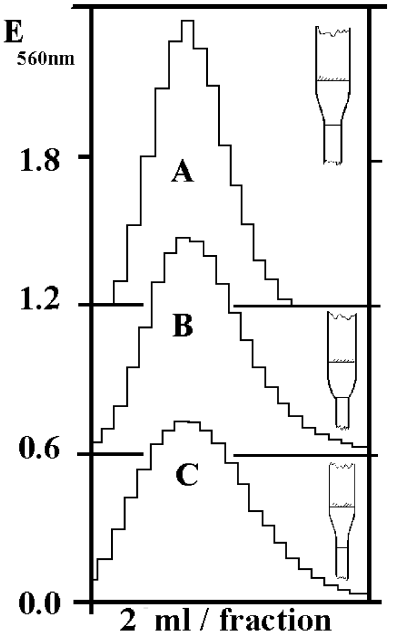


Fig. 4. CFC columns with different variable wall curvatures. A 73-ml volume of soft size exclusion matrix (Sephadex G-25 medium-sized beads) were filled as dense slurry into different shaped conical columns (the shapes used are shown as inserts $2R_1 = 2.5$ cm, $2R_2 = 5$ cm, $h$ varied between 5 and 5.8 cm to give 73 ml) and equilibrated with isotonic salt buffer. Then the upper flow adapter was removed and 2 ml of colored buffer solution were carefully layered on top when the outlet was still closed. The outlet was carefully opened until the color had disappeared. The same method as overlaying was used to wash 3 times with 1 ml buffer. Then the outlet was closed and the buffer was overlaid. The upper flow adapter was put in position and connected to the buffer reservoir to give a pressure of about 0.5 m water columns, then 2 ml fractions were collected. The eluted colored peaks were positioned with their maxima above each other to allow a comparison of the elution profiles. By comparison it is obvious that the wall curvature influences the peak-shape. The column with the smoothest change of curvature (A showed smallest maximal $\varphi$) gave the sharpest peak. This figure is a combination of Figs. 1 and 2 from Ref. [19].

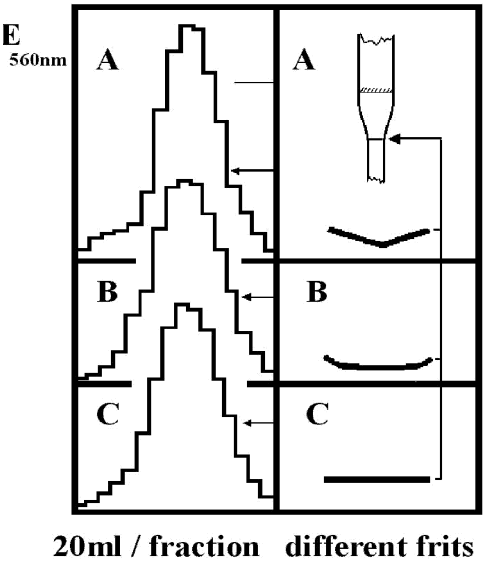


Fig. 5. CFC columns with optimal wall curvatures and differently curved frits at the outlet. A 1000-ml volume of soft size exclusion matrix (Sephadex G-25 medium-sized beads) were filled as dense slurry into smoothly shaped conical columns (the shape used shown as inserts. It corresponds to the shape A shown in Fig. 4: $2R_1 = 5$ cm, $2R_2 = 10$ cm). The column was prepared and run as described above. The difference was that 20-ml fractions were collected and differently curved frits at the outlet were used. Those shapes of frits are shown at the right side of the figure in their cross section. Fig. A gave the best result but showed a little bit too much fronting. Therefore for future work an intermediate shape A and B was chosen, which was a 10-cm diameter cap of a sphere with a height of about 1 cm. (This type of curvature applies only to packed beds of soft spheres. Hard sphere packing as commonly used in HPLC can cause more complicated curvatures and need consequently differently shaped frits for compensation. Those shapes can be found by the same principle as shown here.) This figure is a combination of Figs. 1 and 6 from Ref. [19].

5-cm diameter, which had been suitably modified in a workshop. Details are described in [10,19].

The column itself had a volume of 1 l and an upper diameter of 10 cm. The top of the column was initially left open so that the solution could be applied uniformly across the whole surface, this eliminated the external dispersion as far as possible and we could be sure that the results were mainly due to the different curvatures of the frits at the outlet. The resulting elution profiles for different frit shapes are shown in Fig. 5. Caps of paraboloids gave the best compensation of dispersion for soft packings.

In a patent [20] we showed that the different migration distances in a cone can be partially compensated for by the insertion of a second cone which blocks the direct path of the flow in the center of the separation tube. The bed becomes this way packed between the inside and the outside walls of the two cones. The opening angles of the two cones are equal but the flow is still convergent (Fig. 6E).

Housings with different types of convergence are shown in Fig. 6. A column used for AFC can easily be converted into a CFC column by insertion of a cone (Fig. 6D). Then the same equipment as for AFC can still be used. The advantage is that solid (male) cones are much easier to manufacture than hollow (female) cones. A converging flow is characterized in that the cross section at the inlet is larger than the cross section at the outlet and that the housing does not restrict the flow through the packed bed. (Compare Section A.3 of the Appendix.)

In narrow analytical columns no additional alterations are necessary to upgrade from AFC to CFC to get a better resolution. But the performance can become even better when a curved frit at the outlet is used to compensate for dispersion. Such curved frits improve the performance also for AFC as was shown by Arlt and co-workers [33,34].

Various designs for CFC columns were described [20,35]. Examples of process-scale and of preparative columns are shown in Figs. 7 and 8, respectively.

Both constructions have six common characteristics:

1. A concave frit.
2. A converging column section (bigger area at the inlet than at the outlet) connected to
3. A straight section that allowed flexible volume changes of the packing.
4. A column-head with two independent inlets for fluids, one at the surface of the packing, and one under the roof of the column in the ‘‘dead volume’’. The big space in the column head is a facultative active volume for sample application and sharpening.
5. The upper frit follows the moving surface of the packing as it compresses and expands. In smaller columns the frit is pressed down by a spring, while in larger columns the weight of the frit at the inlet is sufficient to hold it in the correct position.

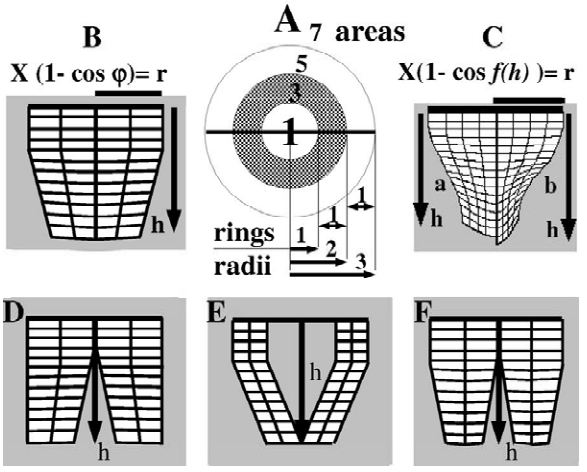


Fig. 6. Different kinds of convergence in CFC columns. (A) Cross section in the cylindrical section of the column with equal-distant flow lines: $r_1 = 1$, $r_2 = 2$, $r_3 = 3$ result in concentric rings, which show a volume relationship of uneven numbers: 1, 3, 5 . . . when perfused by the same flow. In evenly spaced coordinates the outer rings are therefore more important than the central ones. (B) Conical column with constant wall curvature $\varphi$. This figure is the modified Fig.7A of Ref. [20]. (C) Two conical columns with variable wall curvature $\varphi$: a stronger curvature on the right side (b) and a less strong on the left side (a). This figure is the modified Fig. 3 of Ref. [19]. (D) Cylindrical conventional column with inserted solid cone and constant wall curvature $\varphi$. This figure is a modified figure from Ref. [35]. (E) Conical column with constant wall curvature $\varphi$ and equidistant flow-line spacing to compensate for internal dispersion by column shape only. This figure is the modified Fig. 7C of Ref. [20]. (F) Conical column with constant wall curvatures $\varphi$. This is a combination of Fig. B and D above [20,35]. It is important for convergence that only the cross section area at the inlet is bigger than the one at the outlet.

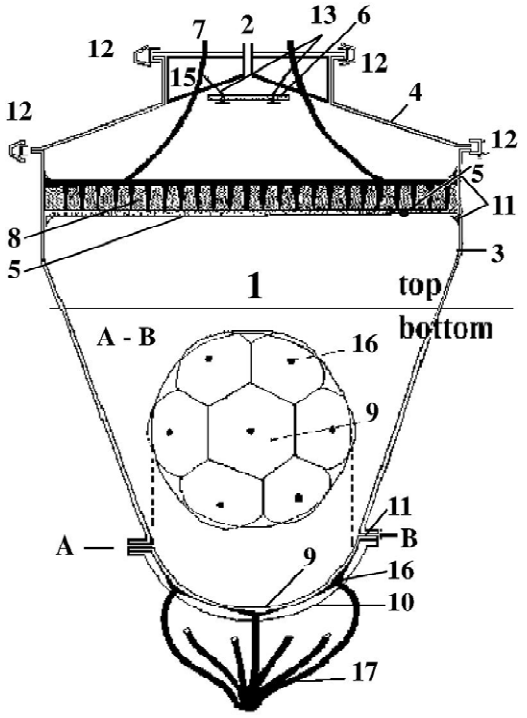


Fig. 7. An example for a process-scale CFC column. 1 = Matrix/filling; 2 = buffer inlet; 3 = confining wall; 4 = lid with conical roof; 5 = flat porous plate, respectively glass fiber filter at the inlet; (6) porous plate used as disperser of buffer; (7) sample inlet; (8) heavy perforated plate (is in Fig. 8 replaced by a spring); 9 = bent metal flies; 10 = separate bottom of column; 11 = sealing, respectively O-ring; 12 = clamp; 13 = holder for disperser; 16 = cone to collect eluate; 17 = flexible tubes of equal length to collect eluate from inner matrix surface at the outlet. This figure is a combination of Figs. 2 (top) and 5 (bottom) of Ref. [20].

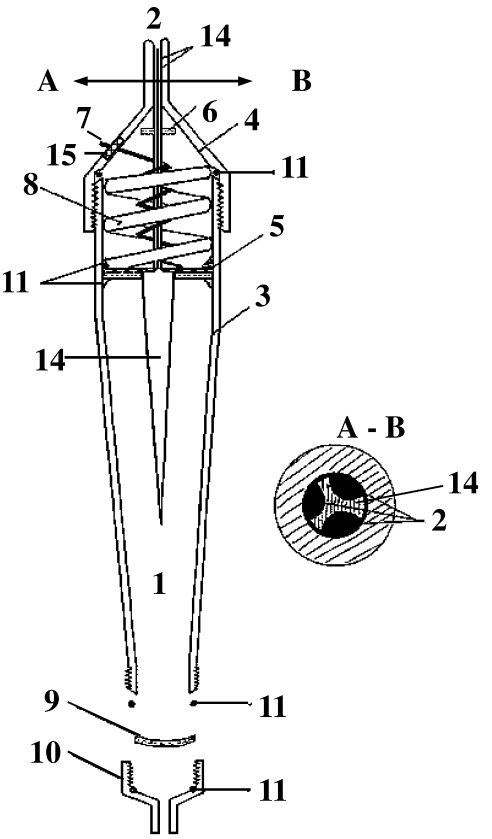


Fig. 8. A preparative CFC column with minimal dispersion. The numbering is in this figure the same as in Fig. 7. 8 = A spring here, which replaces a perforated plate to follow the fluctuations of the surface of the packing; 14 = extension for the arrow-shaped central cone (only in Fig. 8 here); 15 = elastic insert in the upper cap (stopper in Fig. 7, ring in Fig. 8.). This figure is a modified Fig. 4 of Ref. [20].

6. The construction allows uncoupling of the different phases of the separation cycle.

The scheme used for separation (Fig. 9) allows uncoupling of the sample loading and sharpening at low pressure and the separation at high pressure.

1. The outlet is closed and the column is filled using the dead-volume as a sample reservoir. The diluted sample floats to the top and can be removed using an overflow when the reservoir is full. This sharpens the ‘‘back’’ of the peak.
2. The column is compressed by loading of the sample while the outlet is kept closed. A pressure sensor with a contact-switch acts as feedback control for the inlet valve and the pump.
3. The outlet is opened and the elution buffer is automatically topped up, until the set pressure is reached. The process can be regulated by measurement of the following basic parameters: time, pressure, flux, and time dependent energy consumption of pump, conductivity and extinction. Conductivity and extinction are mainly used to switch the valves to collect the different fractions.
4. The regeneration of the matrix is started when the sample is still eluting.
5. After regeneration the column is in this case depressurized to become loaded again. For this it is necessary to wait for approximately 7 min for the packing to relax (expand). A new sample can

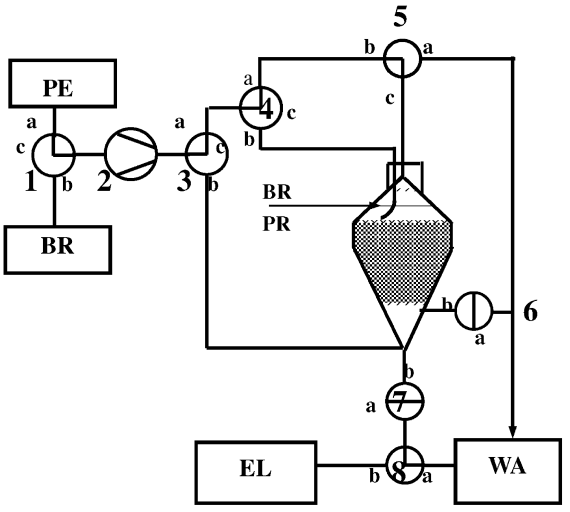


Fig. 9. Scheme of the pressure-controlled CFC process. PE = Probe/sample; BR = buffer; WA = waste; EL = eluate. Five times a 3-way valve (1, 3, 4, 5, 8); 2 times a 2-way valve (6, 7) 1 pump (2). Details of the process can be found in the ''Offenlegungsschrift'' (DE19718652 A1) of Ref. [20] and in the text.

then be applied to the relaxed column and the cycle starts from the beginning.

The relaxation between the cycles is of advantage when one wants to put through a big volume because in the relaxed state the void volume of the packing increases. In the relaxed state the column can be loaded with about twice the volume compared to the compressed state and the danger of shock layer formation is reduced.

The pressure dependent change in the void volume fraction observed by others [36–38] is used here for a more efficient desalting. The big volume changes encountered here are no problem for the self-stabilized bed.

A permanent compression has the advantage that it minimizes the void volume and therewith also the interstitial mixing, which is geometrically the fundamental process of dispersion. The consequences are sharper peaks. This phenomenon can be observed in soft particle packings only and not in hard packings because those particles are not flattened by compaction. By theory soft packings should therefore allow separations with less dispersion than hard packings.

In connection with their mechanical axial-compressed column Baru and co-workers described already in axial compressed AFC such improved separation performance for relative soft Sephadex G-25 (fine) [36] and Bio-Gel P-2 [39].

We developed a special column-head for the automatic processes described above. It has a built-in pressure sensor (Fig. 10) (combination from Refs. [21,22]).

The ''dead volume'' in the column head function as variably buffer reservoir and as the housing for moving parts. It is closed by an elastic cover (number 1 in Fig. 10) that works also as a bumper. The plate and the spring are inside the column head

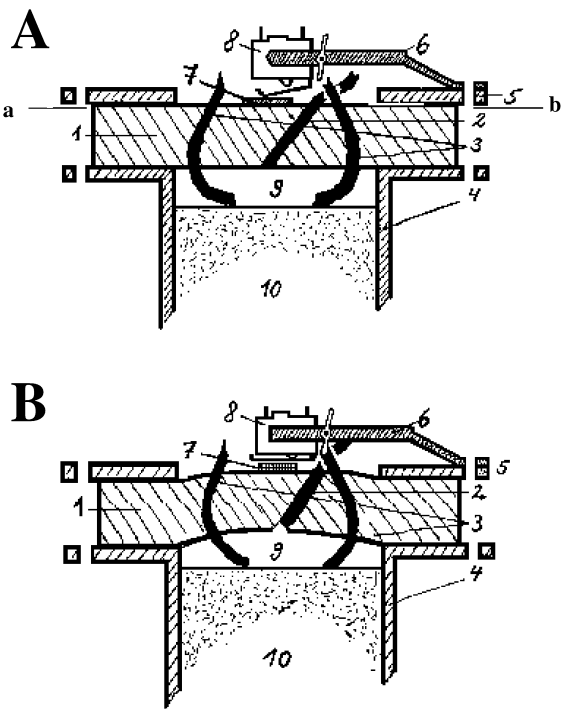


Fig. 10. Multifunctional column head for constant pressure. (A) Column-head is under pressure: flexible cover (1) is bent outside and has closed contact (8). (B) Column-head is in relaxed state: flexible cover (1) is flat and lever has opened contact (8). 1 = flexible cover/bumper; 2 = buffer inlet, overflow outlet to sharpen applied sample; 3 = several flexible tubes for underlying the sample; 4 = confining wall of the lid; 5 = flat annulus to hold the flexible cover in the gasket; 6 = clamp to hold and adjust the distance to the lever of the switch; 7 = distance plate to protect the flexible cover; 8 = switch with lever to make contact; 9 = operation space in column head for sample application (''dead volume''); 10 = matrix/filling. Elements of this figure are found in Refs. [20–22].

(number 8 in Figs. 7 and 8) and deliver only a slight axial pressure necessary to maintain the contact between matrix and the frit at the inlet. The main pressure is brought up externally by the buffer pump. Therefore no moving parts have to be sealed against a high pressure. This is a big constructive advantage compared to other mechanical compressed columns.

We tested a 4-l bed for desalting serum samples (3.2%, w/v, protein in 2 *M* salt at 4 °C, which is a rather viscous solution). In an automatic cyclic manner we went up to the recommended pressure limits and observed pronounced fluctuations in the flow-rate Q (Fig. 11, compare also Table 1 for detailed conditions) [22].

When we take the viscosity (μ) of water, which is at 4 °C 1.57 CP ($10^{-3}$ kg $10^{2}$ $m^{-1}$ $s^{-1}$ $10^{-2}$ = kg $m^{-1}$ $s^{-1}$ $10^{-3}$) and has a density (ρ) of 1 (kg $m^{-3}$ $10^{-3}$) we cannot have made a big mistake for a physiological buffer.

The observations indicate that this column functions also as a viscometer during separation. The highest pressure-drop is observed in a homogeneous converging flow always in front of the frit at the outlet. The fluxes at constant pressure for the isotonic and citric-salt buffer are the result of the flow resistance of the whole system. The dominance of the cross section at the outlet is a function of the opening angle of the cone. (We suppose it is a function of sin $\varphi$ because for $\varphi = 0$ it should correspond to AFC that means it should be equal to 1.)

The flow resistance of the low salt buffer is in principle a combination of viscous and kinetic effects. But the kinetic effects are of no importance here because of the very slow flow we encounter here (see further below for the actual values).

For the determination of solute viscosity in a converging column it is sufficient when only the sample contains the solute. The flux is measured then at the time point the solute of interest leaves the column. In this case relatively small amounts of sample are sufficient for viscosity determination. During the separation there are phases of fast and slow flow. The slowing down of flow is observed directly before and the speeding up after the solute has left the column. When solutes overlap this becomes also reflected in a modulation of the flux, which reflexes the viscosity of the mixed solutes.

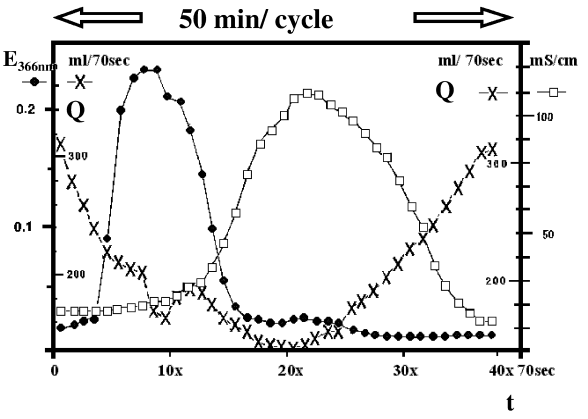


Fig. 11. Desalting of a blood plasma by cyclic CFC in the constant pressure mode at $3 \cdot 10^{5}$ Pa. A 4.5-l column ($2R_1 = 10$ cm, $2R_2 = 17.5$ cm, total bed height of 22 cm therefrom is 2 cm packed matrix in the cylindrical section) packed with 4 l Sephadex G-25 Medium is used to desalt serum samples (3.2%, w/v, protein in 2 *M* salt at 4 °C—which is a rather viscous and sticky solution) in an automatic cyclic manner with constant pressure of $3 \cdot 10^{5}$ Pa at the inlet. The frit at the outlet of 10 cm diameter was made from a circular piece of 13-cm Sika-Fil to let a flat rim for the gasket. The flies had the highest average pore size available of 71 μm. It was made concave (1 cm depth) by pressing with a sphere of 5 cm diameter. In this example we went beyond the flow speeds recommended by the supplier. We measured under physiological salt concentrations (14 mS/cm) a flux of 310 ml/min and with 2 *M* salt (105 mS/cm) a flux of 240 ml/min at the outlet under stable pressure conditions. The protein concentration was measured at the minimum of its extinction profile (366 nm) to avoid dilution errors. Compare for more details Table 1. This figure is a modification of Fig. 3 of Ref. [21].

The borders of the different flow regimes in packed beds are best characterized by the values of their particle Reynolds numbers ($Re_p$). Several authors gave such definition of flow regimes in porous media. Compare for overview Refs. [27,40,42–45].

$$Re_p = Qd_{matrix}/\eta;\ \text{flux: } Q\ (m^3\ s^{-1});$$
$$\text{dynamic viscosity } \eta\ (\text{kg}\ m^{-1}\ s^{-1}) \quad (5)$$

wherein the $d_{matrix}$ must relate to a length of an object of the porous matrix (particle diameter, average pore size, are possible choices). Because different authors have chosen lengths of different objects of the porous matrix there exists a corresponding variety of Reynolds numbers, which differ by a small constant only. Therefore particle Reynolds numbers of different authors may vary by less than one order

Table 1
Data from desalting with CFC in the constant pressure mode (Fig. 11)

| Mode of flux | Equilibrated to constant flux | | Separation with variable flux | |
|---|---|---|---|---|
| Chemical property of fluid | Physiological salt buffer | 2 *M* Tri-potassium citrate | Protein in physiological salt buffer | Low-molecular-mass material in 2 *M* salt |
| Outlet-area $10^{-4}$ m$^2$ | 78.54 | 78.54 | 78.54 | 78.54 |
| Inlet-pressure $10^5$ Pa | 3 | 3 | 3 | 3 |
| Density: ρ kg/l | 1 | 1.01 | 1.03 | 1.06 |
| Particle-diameter 2Rp: $10^{-8}$m | 1.4[b] | 1[c] | 1.3[c] | 1[c] |
| Outlet-porosity $\varepsilon_b$ | 0.15[d] | 0.15[d] | 0.15[d] | 0.15[d] |
| Flux: Mode Q $10^{-3}$ l/s | 5.17 | 4 | 2.5 | 2.42 |
| Flux: Mode G $10^{-7}$ kg m$^{-2}$ s$^{-1}$ | *5.17* | *4.04* | *2.58* | *2.56* |
| Viscosity[a] μ $10^{-3}$ kg m$^{-1}$ s$^{-1}$ | 1.57[a] | | | |

Some of the data have been taken for completion from different sources.
[(a)] Viscosity for water at 4 °C from Handbook of Chemistry and Physics [40].
[(b)] Average wet particle diameter in isotonic buffer [41].
[(c)] Average wet particle diameter in salt buffers from own and other shrinkage data.
[(d)] Porosity at the outlet from extrapolation of observed and reported [36,38] compaction data of Sephadex G-25.

of magnitude, even when they have used the same I.S. system.

Perry et al.'s textbook [40] recommends for porous media Levas' modified particle Reynolds number and corresponding friction factor [46,47]. Between the Reynolds numbers values of 1 and 10 we have Darcy's flow and below 1 creeping flow in this system. The modified particle Reynolds number is defined as:

$$N'_{\mathrm{re\,p}} = 2R_{\mathrm{p}}G/\eta \qquad (6)$$

$R_p$: particle radius (m); $G$: mass flow through cross section (kg m$^{-2}$ s$^{-1}$); $u$: flow-rate (m$^3$ s$^{-1}$); ρ: density: (kg m$^3$); $\eta$: viscosity (kg m$^{-1}$ s$^{-1}$).

From the data of stable buffer flow through the conical column (in Table 2 the first column) we calculated the value for the modified particle Reynolds number (6) as $4.61 \cdot 10^{-12}$. This number lays by the factor of one million beyond that, what was assigned to conventional HPLC as its lower limit by Farkas et al. [48], (compare A.4 of the Appendix for more details).

## 3. Discussion

### 3.1. Viscosity dependent fluxes

The viscosity dependent fluxes in CFC can be explained by the fact that the flow resistance in the cone increases to the same extent as the cross section decreases. Between the cross section and the flow resistance we have an inverse relationship. Therefore

the viscosity of the solute at the outlet limits the flow-rate. This effect becomes more pronounced when the opening angle of the cone is big.

This angle-relationship becomes obvious when one considers that the opening angle of zero degrees corresponds to classical AFC where this effect is not observed at all.

From Fig. 11 we conclude that the elution rate (flux Q = crosses with a connecting dashed line) is inversely related to the viscosity. It is known that the viscosity relates in a non-linear manner to the solute concentrations [49]. The protein is quantified here by extinction and the salt is quantified by its conductivity. The progress of their separation on a converging column can be followed here by the time-dependent fluxes.

When the profile of the flux is compared to the profile of the eluted solutes (protein/salt) they are skewed mirror images of each other with the abscissa as mirror-axis. But there exists a time shift between both profiles, which obscures their connection. This time shift cannot be due to the dead-volume of tubing because it has only a volume of 90 ml, which corresponds to only 0.32 of a fraction when the flux is slowest and it cannot be due to the frit at the outlet because it is wide compared to the packing. This means the flux can be used to follow up the still ongoing separation and is especially reflecting the situation in the cone close to the outlet. This is possible only because the flow resistance is progressively increasing and each solute encounters highest resistant when it comes to the outlet. This progressive increase of resistance is typical for CFC. It is the main difference to RFC where only a linear increase of resistance can be observed and to AFC where no increase is observed at all.

The flow rate of the whole system can become faster only when the first solute starts to leave the outlet and speeds up as soon as higher concentration of the solute start to elute. In our example the size-excluded protein (serum albumin) in fraction 11 is this solute. In fraction 19 the flux increases already before the next solute (in this case it is the salt) comes with its maximum close to the outlet where its flow resistance is highest and starts to elute in fraction 14. But an undisturbed viscosity determination of the pure salt is in this example only possible after other low molecular mass material between fraction 15 and 28 has also eluted and only salt is left over. Its viscosity can be then determined in fraction 30.

The viscosity of the salt can also be determined when the column is completely perfused (first and second column in Table 1) with the same salt concentration. Under such stable conditions one gets only one determination whereas in a separation one gets for each peak many viscosities and related concentrations.

In the desalting example the different fluxes are easily measured. Therefore viscosities of the two solutes we intended to separate can be determined therefrom when Darcy's law is valid. We assume that this is the case, but we cannot prove at this stage that the flux and the viscosity have a simple linear relationship in soft packings. Therefore we want to stop at this stage before this point is clarified.

The dispersion is in RFC and CFC because of the different housing geometry is less pronounced. Both separations have in common that they start with a bigger loading area. Compared to AFC the risk for the formation of a shock layer is therefore considerably reduced. Contradictory to AFC the backpressure increases continuously in both other geometries. The expected increase of flow resistance can be calculated from the relation of outlet to inlet area. In addition the stronger compaction at the outlet of soft packing has to be integrated into the notation of flow resistance.

In RFC the calculated increase is linear because the surfaces of concentric cylinders of equal height relate to each other as do their radii. In CFC the corresponding surfaces are elements of spheres, which relate to each other as the squared radii multiplied by the expression $(1 - \cos \varphi)$ when we consider only a section of the double sphere or a cone.

A high backpressure at the beginning of the separation in CFC is not observed. An increase of pressure is built up later in separation when the solutes migrate down the cone. The flow resistance of a single solute increases to the same extent as the cross section becomes smaller and the bed porosity decreases because of the stronger compaction close to the outlet, which is more obvious for soft packings.

When one considers the backpressure of the whole

system, which corresponds to the total pressure drop one gets backpressure contributions from three sources:

(i) from the viscosity of the carrier solution $_{(buffer)}$
(ii) from the specific viscosities of the different solutes (i) and finally
(iii) from compaction and a denser packing (towards the outlet) $_{(pack).}$

$$\text{AFC: } \Delta p = \Delta p_{buffer}(h) + \Delta p_i\,(h) + \Delta p_{pack}(h) \quad (7)$$

$$\text{RFC: } \Delta p = \Delta p_{buffer} k_r\,(X - X_0) + \Delta p_i k_r (X - X_0) + \Delta p_{pack} k_r (X - X_0) \quad (8)$$

$$\text{CFC: } \Delta P = \Delta p_{buffer} k_c (X^2 - X_0^2) + \Delta p_i k_c (X^2 - X_0^2) + \Delta p_{pack} k_c (X^2 - X_0^2) \quad (9)$$

In conventional AFC constant volume mode the second term becomes normally apparent only under overload conditions [49] and the third term becomes visible in hard sphere packing after ''catastrophic events'', which have often a new packing of the column as a consequence [50]. Whereas in soft sphere packings the third term $\Delta p_{pack}(h)$ is considered because the compaction is finished after a few separation cycles and one works with a relatively consolidated packing [51–59]. In CFC all three terms have to be considered therefore from the beginning, because of the changed geometry all of them contribute significantly to the total backpressure, which regulates the flux in the pressure feed back control we presented here.

### *3.2. Constant-pressure versus constant-volume mode*

Fig. 12 shows schematically the relationship between constant-pressure and constant-volume mode for incompressible fluids in CFC. In constant volume mode an increasing pressure is observed instead of a slower flow. In the constant pressure mode this slowing down is followed by an increased flux. This phenomenon is typical for CFC and cannot be observed in AFC and might be seen in RFC for specific parameter constellations.

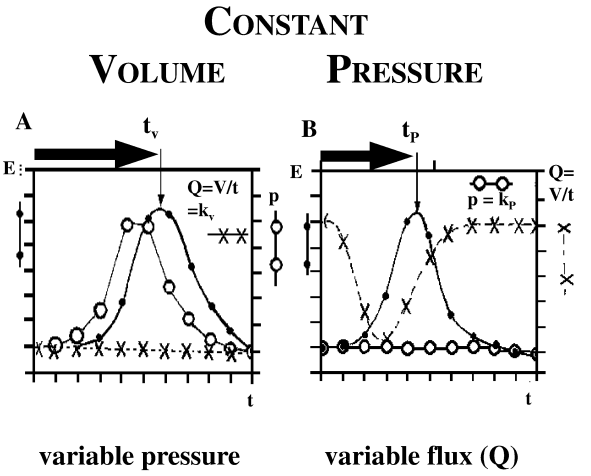


Fig. 12. Schematic comparison of CFC operation in constant volume mode versus constant pressure mode. (A) In the constant volume mode an increase in pressure is observed before the solute starts to leave the conical column (open circles). $t_v$ = the point of elution at constant *v*olume. (B) In the constant pressure mode a drop of the flux $Q = V/t$ ($m^3\ s^{-1}$) is observed when the solute starts to leave the conical column (dashed line with crosses). $t_p$ = the point of elution at constant pressure. The increases of pressure in A and the decrease of flux in B are mirror images of each other with the abscissa as mirror axis. The point of elution ($t_p$) comes in the constant pressure mode earlier than in the constant volume mode ($t_v$) because the cycle times spent in phases without solute are shorter because in these phases the column runs with its maximal possible speed. The big black arrows indicate this difference in elution time. This figure is a modification of Fig. 1 of Ref. [21].

When considering one solute only (Fig. 12B) it is sufficient to concentrate on the cross section area at the outlet and its porosity, because the property of this tightest position of the cone dominates the flow resistance of the whole system. At the time point of slowest elution the maximal concentration of the solute enters the smallest cross section with the tightest packing. Only after the solute has passed this area with its maximum does the flow-rate increase again.

The viscosity of concentrated solutions is a crucial restriction for their separation in preparative chromatographies. This becomes apparent when observing the high variability of flux in CFC in the constant pressure mode. In AFC in the constant volume mode fluctuations of the flow can principally not be

observed directly because they are replaced by pressure fluctuations.

In AFC one observes a more or less constant flow resistance when the cylindrical bed is perfused axially with buffer. The buffer contains in the present praxis of chromatography only diluted solutes and the viscosity of the solutes is normally either neglected or accepted. When using the constant volume mode the consequence is an uneven heating up of the system, which causes problems in separations [9,60,61]. In this situation it is normally not thought about that for the practical application most of the heat could be avoided when the constant pressure mode would be used instead of the constant volume mode.

### *3.3. Bed compaction*

For high concentrated solutions and for suspensions the knowledge of their chromatographic behavior has remained rather fragmentary—despite viscous solutions and suspensions being the most interesting ones for preparative separations. Under overload conditions viscous effects cannot be neglected anymore in AFC. The phenomenon of shock layer formations observed in AFC is the result of the flow impact on the top layers of the packing [62]. It is followed by a slower flow. In the constant volume mode the higher viscosity at the beginning of the separation demands here a higher power input to keep the eluting volume constant against the initial higher backpressure. This can initiate a consolidation in hard and soft packings at the inlet. The formation of such shock layers is facilitated under overload conditions and is accompanied with a locally increased back-pressure. But such layers normally cause only problems when the overload is not only due to high concentration but also to a big volume of the sample. In soft packing the formation of a shock-layer is accompanied by local consolidation of the matrix to a much harder layer compared to the rest of the packing, which can be often reversed only by mechanical removal of the top layer or unpacking of the whole column. Compare also [63]. Otherwise the resistance at the entrance might limit the flow speed of the whole system. This phenomenon of shock-layer formation in preparative columns is well known from analytical gel electrophoresis especially when high viscous samples like high-molecular-mass DNA have to be separated on a porous matrix the situation can become extreme, which is counteracted here by the low voltage used [64]. It is general praxis in electrophoresis to start the separation therefore almost always at a relatively low voltage to avoid shock-layer formation at the gel surface and to increase the voltage not before the sample has entered the gel completely and has migrated some distance. Such information is normally found only in laboratory journals and method-orientated textbooks [65]. By the way in our desalting column we have acted accordingly because we have loaded the column with less pressure than we did the separation with.

When using either kind of packing material for AFC one observes at the beginning of each run an increased back-pressure, which flattens with progression of separation and falls as long solutes leave the column and become successively replaced by buffer. The fading of backpressure is due to different effects: spatial separation in the matrix, diffusion and dispersion. All three effects decrease the local concentration of solutes. The consequence is that the initial high viscosity causes a high backpressure, which fades progressively away because of internal dilution.

When coming from conventional HPLC the next step to more complexity can be the use of soft packings, the application of highly concentrated solutions, the use of different column geometries or the use of a constant inlet pressure. But it is not common to take all these steps at once—as we have done here. Each of these steps needs other equipment and additional concerns and there exists no commercial equipment, which can be used to run such a system.

In the following we want to summarize which types of effects we are aware of from other applications we encounter here. In soft sphere packings an increasing degree of consolidation towards the outlet is observed after simple perfusion in cylindrical packings [51–59]—whereas a corresponding consolidation takes long in hard sphere packing. Such catastrophic events, can be classified as crystallite formation in hard sphere packing and have to be seen as a normal thermodynamic process of aging. Channeling and blockage can be seen on this base as the

same phenomenon. They differ only in their orientation relative to the flow-axis.

### 3.4. Interrelation of shape factors

Leva's correlation is recommended by the latest edition of Perry's Chemical Engineers Handbook [40] for a quantitative description of the flow through a porous media using a modified particle friction factor. This factor is defined as:

$$f_p = 2\,R_p \rho \varepsilon_B^3 \Delta p \Phi_p^{3-\nu} / [2\,G\,2\,h\,(1-\varepsilon_b)^{3-\nu}] \qquad (10)$$

$\Delta p$: the pressure-drop respectively the backpressure when a negative singe is used; $R_p$ the particle radius; $\varepsilon_b$ the bed porosity; $\rho$ the density of mobile phase; $\Phi_p$ the particle shape-factor; $G$ (kg $m^{-2}$ $s^{-1}$) the mass-flux through the packed bed; $n$ for exponential function is varied according to flow regime, which is defined by the Reynolds number (6). From Eq. (10) it becomes clear that the friction is very sensitive towards changes of porosity and the particle shape factor, which both become under compression in soft sphere packing interrelated because the particles flatten. In CFC we are dealing with decreasing cross sections. The cross section area relates to $G$ which is not constant. It is a function of the distance from the outlet ($h$).

From the literature, the void volume fractions ($\varepsilon_p$) given for Sephadex G-25 in the relaxed state is 0.38 [37] and for the compressed state 0.19 [38]. This latter value lies significantly below the value of 0.26, which is the lowest value to be expected for the densest possible packing of equal sized spheres. Newer work using soft particle packings in axial compression columns up to a pressure of 800 kPa confirm these results in separations with mechanical compressed soft packings [36,39]. Compare especially page 21 in Ref. [36].

''Sephadex compression may be supposed to result not only in the rearrangement of the packed bed into a tighter array but also in the deformation of the particles themselves. The latter phenomenon is supported by the decrease in the $V_i$ value and the reversibility of the bed deformation''. ($V_i$ = inner *v*olume in size exclusion chromatography at pressures abo*v*e 200 kPa for wet a*v*erage bead diameters of 52 μm).

Because we used beads with not an average diameter of 52 μm but with a bigger average diameter of 140 μm of the same material, our beads are easier compressed in conical compression as the small beads in a corresponding axial compression. We assumed therefore a porosity of 0.15 for the packing at the outlet an appropriate assumption in our case (Table 1).

This means that the low void fraction observed in compaction can be explained in the following ways. It can be a result of more organized packing with less void space respectively of flattening at the contact areas of the beads. In addition one has to expect in our case that the compaction is strongest close to the outlet, what was not considered by these authors but described by others [51–59]. Under the described pressure the soft particles have no other choice but to adopt polyhedral [66–68] and Voronoi shapes [69].

A further contribution to the chromatographic resistance not included yet in our considerations is the phenomenon of particle segregation. The particle property dependent segregation is known also as the Brazilian nut problem (=BNP) and has become basically understood [70–73]. This basic knowledge should become applied in column packing to improve chromatographic applications in future.

### 3.5. New column head

When the new column heads are used CFC combines the advantages listed below. The dead volume of the new end pieces thus does not cause mixing—in contrary they enable

(i) Uncoupling of the different cycle phases,
(ii) damping of fluctuations,
(iii) measurement of pressure,
(iv) automatic pressure-dependent switching,
(v) sample under-laying and therewith an even sample distribution over large cross sections, which abolishes all dispersions normally observed in distributors at the inlet,
(vi) peak sharpening,
(vii) automatic movement with the surface of the packing.

The synergetic combination of the modifications—which we developed for CFC but are also partially applicable to AFC and RFC—allow shorter cycle periods, a more efficient utilization of the separation matrix and less wear to the filling and the apparatus.

### 3.6. Minimizing dispersion

CFC is superior to AFC and RFC because the converging flow minimizes band spreading. This is simply explained.

When separation commences, a sample of high concentration is spread over a large area. In the region where the flow speed is low, the stationary phase is used efficiently as the solutes have more time to interact with the stationary phase. With the progression of the solution through the matrix, the cross section of the cone reduces and the flow is accelerated. Thus, the probability of interaction further down in the cone—where the compounds have already separated from the bulk—is drastically reduced. Also the number of voids and their size is decreasing. They provide the space where dispersion happens by mixing and dilution. This way unnecessary dispersion can be avoided when almost all the material has become separated already. Finally the stage is reached when only the slowest compounds remain. If their concentration is small, they are less susceptible to further dilution than they would be in other chromatographic systems. Vovk et al. described precisely this beneficial effect (narrower peaks of low intensities when eluting late [18]) for their conical column.

### 3.7. Systematic overview of CFC advantages in the constant pressure mode

Converging flow minimizes band spreading, which results in

(i) sharper peaks,
(ii) less use of matrix,
(iii) less consumption of buffer,
(iv) faster separations with shorter cycle times and
(v) less cross-contamination/better resolution especially for late eluting solutes.

Constant pressure control at the inlet by self-contained robust feedback loop: power input only when it results in fluxes, thus

(i) avoiding internal heat development due to friction and leading to
(ii) more stable separation conditions,
(iii) to measure viscosity by the fluxes respectively by the power inputs,
(iv) to control separations without use of additional sensors,
(v) to reduce stress on the sample, matrix and equipment,
(vi) to separate highly concentrated solutes and even suspensions,
(vii) no need to repack the column, and
(viii) facile automation.

The combination of convergence and constant pressure at the inlet results in a

(1) direct and steady impact on particles:
  (i) no need for additional sealing and mechanical transmission,
  (ii) inexpensive external mechanical devices and
  (iii) minimizing internal heat development,
  (iv) allows internal stabilization of packed beds by
  (v) increasing compaction in direction towards the outlet minimizes: interstitial volumes and therewith the dispersion in soft packings, inter-column variances and makes larger columns diameters manageable.
  (2) Reduces costs of the whole process.
  (3) It allows an easy handling of many columns in parallel. This makes it especially suitable for automation with easy extendable capacity.
  (4) It is able to handle solutions of extreme viscosities (-even crystal suspensions can be separated).

The listed advantages make CFC in the pressure regulated operation mode competitive to all cyclic and continuous chromatographic operation processes. Because of its higher complexity CFC provides more possibilities for optimization compared to AFC and RFC and should allow therefore tailoring a process more exactly. Due to its intrinsic advantages CFC should become recognized to be superior to AFC and RFC.

## Acknowledgements

I thank my son Wofdietrich who checked the English and made me aware of unclear passages in the first version of this paper.

This work was supported by BIOWEST (Nuaille, France) and by the Patent Center of the Fraunhofer Gesellschaft in Munich Reference Number 29551.

Table 2
Unit-volumes of different chromatographies

| | | | |
|---|---|---|---|
| AFC<br>Fig. 1 | Annular<br>cylinders | $V_a = \pi(X_1^2 - X_0^2)\,(h_1^1 - h_0^1)\,(1 - \cos\varphi)$<br>$= \kappa_a\, X_1^2\, h\, 1$ | $X$ = constant<br>$h$ = variable<br>$\varphi^* = \cos 90° = 0$ |
| RFC<br>Fig. 2 | Annular<br>cylinder | $V_r = \pi(X_1^2 - X_0^2)\,(h_1^1 - h_0^1)\,(1 - \cos\varphi)$<br>$= \kappa_r\,(X_1^2 - X_0^2)\, h$ | $X$ = variable<br>$h$ = constant<br>$\varphi^*$ = const. |
| CFC<br>Fig. 3 | Double<br>sphere<br>sector | $V_c = 4\pi/3(X_1^3 - X_0^3)\,(1 - \cos\varphi)$<br>$= \kappa_c\,(X_1^3 - X_0^3)$ | $X$ = variable<br>$\varphi^*$ = constant |
| $CFC_v$<br>Fig. 3E<br>Fig. 6C | Double<br>sphere<br>sectors | $V_{cv} = 4/3\pi(X_1^3 - X_0^3)(1 - \cos[f(h)]^*)$<br>$= \kappa_{cv}\,(X_1^3 - X_0^3)(1 - \cos[f(h)]^*)$ | $X$ = variable<br>$\varphi^* = f(h)$ |

*$\varphi$ is half the opening angle at the center of the double sphere(-s) and determines the wall curvature.

## Appendix A

### *A.1. Classification of chromatographies according their flow geometry*

Rhee et al. described for chromatography in total three types of geometries [1] but did not distinguish verbally radial flow chromatography (RFC) from converging flow chromatography (CFC). He named them together radial chromatographies, but described them separately mathematically. The first with

Table 3
Variables and dimensionless parameters

| Symbol | AFC | RFC | CFC | $CFC_v$ |
|---|---|---|---|---|
| $\tau$ | $\frac{t\,u}{h}$ | $\frac{t\,Q}{V_b\varepsilon_b}$ | $\frac{t^2\,D}{V_b\varepsilon_b\,(1-\cos\varphi)}$ | $\frac{t^2\,D}{f(V_b)\,\varepsilon_b\,(1-\cos f[h])}$ |
| $\varsigma$ | $\frac{Z}{h}$ | $\frac{(X^2 - X_0^2)}{(X_1^2 - X_0^2)}$ | $\frac{(X_1^3 - X_0^3)(1-\cos\varphi)}{(X_1^3 - X_0^3)(1-\cos\varphi)}$ | $\frac{(X^3 - X_0^3)(1-\cos f[h])}{(X_1^3 - X_0^3)(1-\cos f[h_1])}$ |
| $\varsigma_0$ | $\frac{h_0}{(h_1 - h_0)}$ | $\frac{X_0^2}{(X_1^2 - X_0^2)}$ | $\frac{X_0^3\,(1-\cos\varphi)}{(X_1^3 - X_0^3)(1-\cos\varphi)}$ | $\frac{X_0^3\,(1-\cos f[h_0])}{(X_1^3 - X_0^3)(1-\cos f[h_1])}$ |
| $\alpha$ | $1(\varsigma+\varsigma_0)^{1/1}$<br>$[(1+\varsigma_0)^{1/1}$<br>$-\varsigma_0)^{1/1})]$ | $2(\varsigma+\varsigma_0)^{1/2}$<br>$[(1+\varsigma_0)^{1/2}$<br>$-\varsigma_0)^{1/2})]$ | $3\,(\varsigma+\varsigma_0)^{1/3}$<br>$[(1+\varsigma_0)^{1/3}$<br>$-\varsigma_0)^{1/3})]$ | $\Sigma\,3\,(\varsigma+\varsigma_0)^{1/3}$<br>$[(1+\varsigma_0)^{1/3}$<br>$-\varsigma_0)^{1/3})]$ |
| $\Pi_i$ | $\frac{\varepsilon_p^2 D_{ip}\, h}{R_p^2\, u}$ | $\frac{\varepsilon_p^2 D_{ip}\, \varepsilon_b V_b}{R_p^2\, Q}$ | $\frac{\varepsilon_p^2 D_{ip}\, \varepsilon_b\, V_b\, t}{R_p^2\, D}$ | $\frac{\varepsilon_p^2 D_{ip}\, \varepsilon_b t\, f(V_b)}{R_p^2\, D}$ |
| $Bi$ | $\frac{K_f\, R_p}{\varepsilon_p^2\, Di_p}$ | same for<br>hard particles | same for<br>hard particles | same for<br>hard particles |
| $\xi$ | $\frac{3Bi\,(1-\varepsilon_b)\,\Pi}{\varepsilon_b}$ | same for<br>hard particles | same for<br>hard particles | same for<br>hard particles |
| $r$ | $\frac{R}{R_p}$ | same for<br>hard particles | same for<br>hard particles | same for<br>hard particles |
| $Pe$ | $\frac{u\,(h - h_0)}{D}$ | $\frac{u\,(X_1^1 - X_0^1)}{D}$ | $\frac{u\,(X_1^2 - X_0^2)(1-\cos\varphi)}{h\,D}$ | $\frac{u(X_1^2 - X_0^2)(1-\cos f[h_1])}{hD}$ |
| Coord-<br>inate | $(h_1^1 - h_0^1)$<br>$(h - h_0)$ | $(X_1^2 - X_0^2)$<br>$(X_1^1 - X_0^1)$ | $(X_1^3 - X_0^3)(1-\cos\varphi)$<br>$(X_1^2 - X_0^2)(1-\cos\varphi)$ | $(X_1^3 - X_0^3)(1-\cos f[h_1])$<br>$(X_1^2 - X_0^2)(1-\cos f[h_1])$ |

(RFC) cylindrical coordinates and the second with (CFC) spherical coordinates. In our opinion this caused some confusion and hindered the development of CFC. In two personal communications we emphasized this problem [73,74].

The flow of AFC is parallel to the symmetry axis, whereas that of the RFC is in the direction towards this axis ($h$). When using the same coordinates the variable and constant parts are only exchanged (compare Table 2). It makes therefore in the second case no sense any more to talk about linear flows and velocities because the flow is now radial. In CFC the flow is also radial but is not orientated towards a central axis but towards the central point of a concentric double sphere. CFC has compared to RFC one more dimension of convergence.

This approach of induction going from simple forms to the more complicated ones, which was suggested by Rhee et al., we want to use here in the appendix to derive the parameters of CFC from the available information existing about AFC and RFC. The problem we are confronted with is that the more complex CFC has more variables and cannot be completely determined by the simpler forms. But it is clear on the other hand that the more general CFC should include the simpler AFC and RFC as special cases. That means the general notation should describe all chromatographies. The new constants have then successively to be experimentally confirmed or corrected.

With Gu we discussed the first steps to a more detailed description of CFC [73] starting with the chromatographic parameters he had reported for RFC in comparison to AFC [26]. With Prosek we discussed that a truncated cone can be seen as the Unit-element of a concentric double sphere [74].

The step from RFC to CFC is analog in going from AFC to RFC, which corresponds to an increasing complexity of the perfused confinements. In both cases this is accompanied by an increase in the number of variables to be considered. But one can look at this integration also in a simple exchange of constants and variable parts of the equations.

Gu et al. [26] initiated with their Table 1 the theoretical considerations described here. We have adopted their values but generalized their notations. The individual transformations that we have made can be traced back to the underlying geometries with their volume unit-elements. By the complete notations given by us in Table 2 it becomes now more obvious that AFC and RFC are special cases of CFC.

The unit-volume of AFC is normally seen as $V_A = \kappa_A X_1^2\, h$. But this is a special case of the double-cylinder. The double-cylinder and not the simple cylinder is the basic element of AFC (Fig. 1). This shows the experiment and the theory.

A cone with a small opening angle can be seen in CFC as a unit-element of the double-sphere. Because $\varphi$ is constant here it can be combined with the spherical constants, the constant $\kappa_c$. But the $\varphi$ of CFC can also be a variable that depends on the wall curvature of the chosen column. For big opening angles of columns the exact geometrical description should be used because the volume of the truncated cone becomes then too different from the sector of a double sphere. For illustration compare $X$ and $X'$ in Fig. 3B and C.

### *A.2. Chromatographic parameters for different flow geometries*

After we have compared the unit-elements of the different chromatographies, we want to show now in Table 3 how they become reflected in the chromatographic parameters.

For $\tau$ we have the information that $tv/h$ $[s \cdot m/(s \cdot m)]$ of AFC transforms in RFC to $tQ/(V_b \varepsilon_b)$ $[s \cdot m^3/(s \cdot m^3)]$. Therefore we look in CFC for something like $[s \cdot m^5/(s \cdot m^5)]$ or $[s^3 \cdot m^3/(s^3 \cdot m^3)]$. Our suggestion is: $t^2\, D/(V_c\, \varepsilon_b\, (1 - \cos\varphi))$ $[s^2\, m^3/s^2\, m^3]$.

This dimensionless parameter combination could give information on the dispersion in dependence of quadratic time progression of separation in the cone after entering the packed bed by solutes, which is of real interest for description of CFC's flow.

$\alpha$ was written for AFC in its general notation in a way that it became similar to RFC. Then it was assumed that the step from AFC to RFC is analog to the one from RFC to CFC. By this induction we came to a new $\alpha$ for CFC.

In those cases where the unit-elements in AFC and RFC were recognized, they were replaced by unit-element of CFC without considerations.

When no change was observed by going from AFC to RFC [26], we cannot expect a change by going from RFC to CFC either. Therefore we have said also ''same '' as GU et al. did in their Table 1.

But one should be aware that their parameters concern only hard particle packings. Therefore we have extended their ‘‘same’’ every where by ‘‘for hard particles’’. This makes it clear that a whole lot of parameters might differ in hard and soft packings.

The Peclet number in CFC gets by the induction one more length dimension, which needs to be balanced by a different length in the nominator. We suggest *h* for this purpose, which is the distance to the outlet along the symmetry axis. But, of course, other lengths could be chosen as well.

In the present state the values given in Table 3 are only tentative and need an experimental proof and according corrections. Using this inductive theoretical approach lets us get a better idea, what we have to expect from the new chromatography. This allows us to focus better on the clarifying experiments.

### *A.3. Definition of convergent flows*

In Fig. 6 different types of housings for convergent flows are shown. In Fig. 6A a circular cross section is divided by equal spaced concentric circles. The corresponding areas of the rings increase by uneven numbers. But when the radii increase with the radix of natural numbers instead the concentric rings get all the same the area as it is sketched in Fig. 13A.

When one is now dividing the cross section by two diagonals all the different ring-sections between the arrows represent then the same area. When one connects now any two areas of a ring from a different cross section with each other (two possibilities are shown here in this figure) and is looking now on the cutting-plane of the cylinder from the side (Fig. 13B) some shapes seem to diverge whereas others seem to converge despite all the cross sections having the same area and the shown shapes therefore are neither converging nor diverging.

In reality a convergence in one direction is compensated by another divergence in a different direction. When a flow has to perfuse such structure it must move in the plane. That means it is accelerated. In our slow flow this effect can be therefore most probably neglected.

This geometrical example shows how difficult it is to judge by the seen angles of the containment whether a shape is diverging or converging. Consequently it is always necessary to determine the area

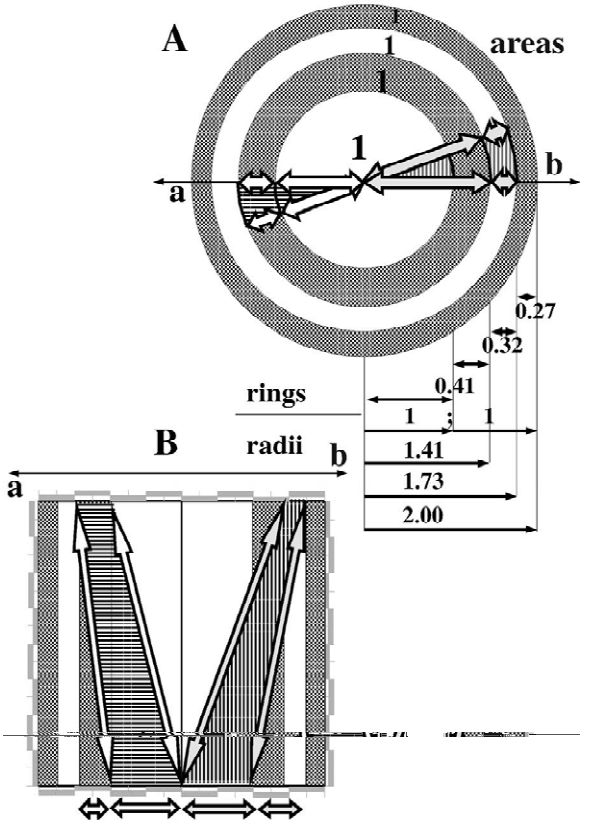


Fig. 13. Defining convergence and divergence by the areas of the inlet and outlet of the perfused confinement. (A) Cross section in the cylindrical area of a CFC column with equal-area flow lines: $r_1 = 1$, $r_2 = 2^{1/2} = 1.41$; $r_3 = 3^{1/3} = 1.73$ result in concentric rings, which show a 1:1 relationship of areas. When they are perfused their fluxes will also show this 1:1 relationship. The rings become in this arrangement continuously closer spaced towards the periphery. In evenly spaced coordinates the outer rings covered a bigger area than the central ones (Fig. 6A), here they cover all the same area. They are labeled by shading between the arrows on the different rings. (B) The section along the main flow (indicated by the double-headed arrows and the areas shaded with parallel lines in between) cut flows, which do not change their cross section area but only its shape. All the shown flows are neither convergent nor divergent. They demonstrate that the boundary between convergence and divergence can be defined only on the base of cross section areas.

of the perfused cross sections at the inlet and the outlet before one can decide whether one is dealing with a diverging or a converging flow. In addition one might have to introduce a factor for the lateral displacement of the flow, which is determined by the housing geometry. This factor must conform with the form factors summarized by Carman in 1937 [75].

*A.4. Theoretical considerations to very slow flow regimes encountered in chromatography*

The porosity in Leva's friction factor (10) is exponentially dependent on the size of the actual Reynolds numbers (6). This means the exponent approaches the value of 3 the slower the flow becomes. It is disputed how far below 1 the value of Darcy's flow reaches [27,48]. That means to which value of Reynolds number a linear inverse relationship between flux and viscosity reaches. The relationship to the exponent given by Leva ends abruptly for $n = 1$. Leva and others classify everything below this value as laminar flow. But his scale of Reynolds numbers is extending only to $10^{-3}$.

$$N^{a}_{\mathrm{re}\ p} = 10^{-6},\ n = 0? \tag{11a}$$

$$N^{b}_{\mathrm{re}\ p} = 10,\ n = 1 \tag{11b}$$

$$N^{c}_{\mathrm{re}\ p} = 100,\ n = 1.7 \tag{11c}$$

$$N^{d}_{\mathrm{re}\ p} = 1000,\ n = 1.94 \tag{11d}$$

Leva did not define the corresponding exponent of the friction factor in this region; despite his plot of $n$ looks like it was artificially stooped at a value of 1. We suspect that for (5a) $N^{a}_{\mathrm{re}\ p} = 10^{-3}$ $n$ might reach 0.5 and for $N_{\mathrm{re}\ p} = 10^{-6}$ it finally might reach $n = 0$.

For this area of flow regime there exists very few measurements in the literature. From investigations on AFC [48] we know that the lower limit of the flow regime for conventional hard sphere packing ends with a value of about $10^{-6}$ for the particle Reynolds number. In this area linear inverse relationship between flow and viscosity was shown to be valid. In our case the value for the Reynolds number lies by a factor of 1 million below the lower limit given by Farkes et al. [48].

When our assumption (11a) would turn out to be correct this would allow us to simplify the resistant factor (10) to:

$$f_{\mathrm{p}} = \Delta p\ R_{\mathrm{p}} \rho \Phi_{\mathrm{p}}^{3}\ \varepsilon_{\mathrm{b}}^{3} / [G\ 2\ h\ (1 - \varepsilon_{\mathrm{b}})^{3}] \tag{12}$$

and the following rearrangement becomes possible because the exponents now fit better to each other:

$$f_{\mathrm{p}} = \Delta p\ R_{\mathrm{p}} \rho [\Phi_{\mathrm{p}} \varepsilon_{\mathrm{b}} / (1 - \varepsilon_{\mathrm{b}})]^{3}\ [G\ 2\ h]^{-1} \tag{13}$$

This expression contains $\Phi_{\mathrm{p}}$,$\varepsilon_{\mathrm{b}}$ and $(1 - \varepsilon_{\mathrm{b}})$, which have now got all the same exponent. In our opinion this makes sense because those parameters become under compression geometrically linked. The quotient $\varepsilon_{\mathrm{b}}/(1 - \varepsilon_{\mathrm{b}})$ can be interpreted as the probability to find a pore divided by the probability not to find none.

The alternative is we stick for now to the lower limit of $n = 1$ presented by Leva (5b) which is not as simple and we feel less comfortable with:

$$f_{\mathrm{p}} = \Delta p\ R_{\mathrm{p}} \rho^{*} \Phi_{\mathrm{p}}^{2}\ \varepsilon_{\mathrm{b}}^{3} / [G\ 2\ h\ (1 - \varepsilon_{\mathrm{b}})^{2}] \tag{14}$$

On the basis of our suggestion (12) one has to clarify now with further experiments the situation for very slow flows. We think it will be crucial for these experiments that the measurements cover several orders of magnitude to allow us to test whether there exists a small drift in the exponent such that it reaches finally almost 3.

Let us accept for now Eq. (13). This equation means nothing more than that the flow resistant is mainly dependent only on the ratio of open $\varepsilon_{\mathrm{b}}$ to the closed area $(1 - \varepsilon_{\mathrm{b}})$. This quotient is dominating the whole expression because it goes in by power three whereas all other parameters have only a linear influence except the particle shape factor $\Phi_{\mathrm{p}}$, which goes in with the same exponent. The quotient and $\Phi_{\mathrm{p}}$ should become in soft particle packing directly related when the packing is compressed. But the exact shape of the compressed particles will depend on their packing geometry. We know neither their geometries nor the border conditions these shapes depends on.

In this context it was not considered yet that the quotient of the open $(\varepsilon_{\mathrm{b}})$ to the closed area fraction $(1 - \varepsilon_{\mathrm{b}})$ can be interpreted as an exponential function. After approximation one finds

$$\varepsilon_{\mathrm{b}}\ (1 - \varepsilon_{\mathrm{b}})^{-1} = 2.64 \varepsilon_{\mathrm{b}}^{1.38};\ 0 < \varepsilon_{\mathrm{b}} < 0.5 \tag{15}$$

which covers all porosities found in packed beds.

This expression inserted in Eq. (13) gives (one can insert this expression also in Eq. (14)):

$$f_{\mathrm{p}} = \Delta p\ 2.64\ R_{\mathrm{p}} \rho \Phi_{\mathrm{p}}^{3}\ [2G\ h]^{-1} \varepsilon_{\mathrm{b}}^{4.38} \tag{16}$$

Eq. (16) shows much more clearly than Eq. (13) before the very strong power-dependence on the open area $\varepsilon_b$ in the very slow flow regime.

Despite this suggested notations in the present stage are very tentative and need for their final proof experimental verification, I think this is the most precise way to specify what one has to look for in theoretical clarification of very slow flows, which is still an unexplored field.

We can say in addition that we will have to describe in the notations for the converging flow also the geometry, degree and anisotropy of consolidation, which becomes most obvious in the packed bed at the outlet in soft packings.

The porosity will therefore most probably show a power dependent unisotroph behavior of compaction in addition to the expected dependence by power 4.38 on the packing porosity. When investigating the very slow flows of CFC it will become necessary to transform $G$ to a function, which reflects the geometrical change of the cross section used in each case.

Using Leva's equation we calculated a particle Reynolds number of $4.61 \cdot 10^{-12}$ which lays twelve orders of magnitude below 1 normally assigned to Darcy's flow and still six orders below the lower limit assigned to conventional chromatography using hard sphere packing.

This outcome of the calculations was a surprise for us and we questioned whether we might have made a mistake. Therefore we calculated for control purposes the value of the Reynolds number (6) from the flow data given for conventional chromatography [48] as: 2*Rp*: *10* μm; *Q*: *0.5* ml $min^{-1}$; $\mu$: *20* cP; $\rho$: 1.11 g/ml; $\Delta p$: 144 bar; $u$: 0.08 m $s^{-1}$; 20 °C.

The data in italics were used for calculations only, they gave a value of $2.78 \cdot 10^{-6}$, which corresponds closely to the value of the lower limit of conventional chromatography in hard particle packings given by the authors as $1.7 \cdot 10^{-6}$.

One can conclude therefrom that the limits of the flow regime we calculated for CFC in soft sphere packing lies really by the factor of one million beyond that encountered in conventional chromatography using hard sphere packing.

Even under these extreme conditions the flow is in soft sphere packing not completely blocked and separations are despite strong compression still being possible.

It became obvious that the flux in soft packings of CFC under compression is very sensitive and inversely dependent on the porosity. From extrapolations of the resistant factor to very slow flow regime. We expect that the flattening of the soft spheres will also contribute to a further increase of the resistant factor.

The numerical contribution of this flattening needs experimentally to be clarified. Another question, which stays in close context to the particle shape factor, is the question of the influence of the particle size homogeneity on segregation, on packings and on the resulting flows and separations. The real question to be clarified in future will be most properly: whether the observed flux modulation in our system is more due to time-dependent viscosity or porosity respectively, and to a combination or interplay of both.

One can put the last question differently. What do we really measure in soft packings of CFC in constant pressure mode bed compaction or viscosity bridging?

## Appendix B

### *B.1. Nomenclature*

#### *B.1.1. Variables*

| | |
|---|---|
| D | dispersion ($m^3$ $s^{-2}$) |
| $D_i$ | effective diffusity of component (solute) i ($m^2$ $s^{-1}$) |
| $G$ | fluid mass velocity based on the empty cross section = distance kg's moved in time down in a container (kg $m^2$ $s^{-1}$) |
| $h$ | coordinate in direction of symmetry axis, distance to outlet (m) |
| $\eta$ | dynamic viscosity (kg $m^{-1}$ $s^{-1}$) |
| $\nu$ | cinematic viscosity = $\eta/\rho$ ($m^2$ $s^{-1}$) |
| $P$ | Poise (unit of dynamic viscosity) (g $cm^{-1}$ $s^{-1}$) |
| Pa | unit of pressure Pascal ($=10^{-5}$ bar) (N $m^{-2}$) |
| $Q$ | flux of the mobile phase ($m^3$ $s^{-1}$) |
| $R$ | radius of packed bed (m) |
| $R_P$ | particle radius (m) |

| | |
|---|---|
| S | Siemens (unit of electrical conductivity) ($A\,V^{-1}$) |
| St | Stokes (unit of cinematic viscosty $\nu$) ($cm^2\ s^{-1}$) |
| $t$ | time (s) |
| $t_v$ | elution time in constant volume mode (s) |
| $t_p$ | elution time in constant pressure mode (s) |
| $u$ | superficial (apparent) velocity in filled containment ($m\ s^{-1}$) |
| $u_v$ | void (interstitial) velocity ($m\ s^{-1}$) |
| $V_0$ | exclusion, respectively void, volume of packed bed ($m^3$) |
| $V_b$ | bed volume ($m^3$) |
| $V_i$ | inner accessible particle volume for solute i ($m^3$) |
| $V_t$ | elution volume of solute ($m^3$) |
| $\rho$ | density ($kg\ m^{-3}$) |
| $X$ | radial coordinate of container/packing (m) |
| $Z$ | axial coordinate of containment/packing (m) |

*B.1.2. Dimensionless constants*

| | |
|---|---|
| $\alpha$ | $(\varsigma+\varsigma_0)$ (Table 3) |
| $Bi$, $K_f\ Rp/\varepsilon_p^2 Di_p$ | Biot number (mass transfer) (Table 3) |
| $\varepsilon_b$ | fraction of pores in bed (voids, interstices), bed porosity |
| $\varepsilon_p$ | fraction of pores in particle, particle porosity |
| $H$ | units of containment length in direction of symmetry axis |
| $\Pi_i$ | (particle pore accessibility for solutes i) (Table 3) |
| i | component, solute |
| $\varphi$ | half opening angle of element of double sphere (cone) |
| $\kappa_{cv}$ | $4\pi/3$ volume constant of sphere (Table 2) |
| $k_{f\,i}$ | Mass transfer film factor of solute i |
| $\Phi_c$ | packing form-factor: surface/volume of containment |
| $\Phi_p$ | particle form-factor: surface/volume of particle |
| Pe | Peclet number (derivation from plug flow) (Table 3) |
| $\varsigma$ | unit of volume: actual ($V$)/bed volume ($V_b$) (Table 3) |
| $\varsigma_0$ | unit of volume: actual ($V_0$)/bed volume ($V_b$) (Table 3) |
| $r$ | units of particle-radii distance (Table 3) |
| $\tau$ | tortuosity: real flow length/shortest distance of flow (Table 3) |
| $\xi_i$ | $3Bi(1-\varepsilon_b)\eta/\varepsilon_b$ (Table 3) |
| $Re_p$ | particle Reynolds Number (flow regime in packed beds) |
| $N'_{Re}$ | leaves modified particle Reynolds number: $2R_pG/\eta$ |
| $f'_m$ | (flow resistant) friction factor modified according to M. Leva |
| $n$ | exponent in friction factor ($f'_m$) as function of $N'_{Re}$. $N'_{Re}=10^{-1}$, $n=1$; $N'_{Re}=10^{-2}$, $n=1.7$; $N'_{Re}=10^{-3}$, $n=1.94$; $N'_{Re}=10^{-4}$, $n=2$; $N'_{Re}=10^{-6}$, $n=3$ suggested extrapolation for very slow flows as encountered in chromatography. |

## References


[1] H.K. Rhee, R. Aris, N.R. Amundson, Philos. Trans. R. Soc. Lond. A 267 (1970) 419.
[2] Announcement of ''100 Years of Chromatography'', 3rd International Symposium on Separation in the BioSciences, Moscow, 13–18 May 2003.
[3] J.P. Knox, J.F. Parcher, Anal. Chem. 41 (1969) 1599.
[4] E. Sada, S. Katoh, M. Shiozawa, Biotechnol. Bioeng. 24 (1982) 2279.
[5] T. Yun, G. Guichon, J. Chromatogr. A 672 (1994) 1.
[6] M. Perut, J. Chromatogr. A 658 (1994) 293.
[7] H. Kubota, M. Ikeda, Y. Nishimura, Kagaku Kogaku Ronbun 298 (1965) 611.
[8] T. Farkas, M.J. Sepaniak, G. Guichon, AIChE J. 43 (1997) 1964.
[9] O. Dapremont, G.B. Cox, M. Martin, P. Hilaireau, H. Colin, J. Chromatogr. A 796 (1998) 81.
[10] W. Pfeiffer, Pat. DE9317551.5 (16 Nov. 1993; 27 Jan 1994).
[11] A.S. Said, J. High Resolut. Chromatogr. Commun. 2 (1979) 63.
[12] A.S. Said, Theory and Mathematics of Chromatography, Hüthig Heidelberg, 1981, p. 155.
[13] V.R. Deiison, I.A. Favorskaja, Z.A. Sevencko, Pat. SU105531A (5 Aug. 1982).
[14] M. Prošek, A. Pečavar, A. Medja, Pat. SLO 9300206A (20 April 1993).

[15] M. Prošek, A. Golc-Wondra, A. Pečavar, I. Vovk, 14th International Symposium on Capillary Chromatography, Riva del Garda, 1994, p. 1568.
[16] A. Pečavar, A. Smidovnik, M. Prošek, Anal. Sci. 13 (1997) 229.
[17] A. Pečavar, L. Vovk, J. Marsel, M. Prošek, Anal. Sci. 15 (1999) 233.
[18] I. Vovk, A. Pečavar, M. Prošek, J. Planar Chromatogr. 12 (1999) 66.
[19] W. Pfeiffer, Pat. DE4440805C2 (16 Nov. 1993; 26 Nov. 1998).
[20] W. Pfeiffer, Pat. DE19718652C2 (3 May 1996; 20 July 2000).
[21] W. Pfeiffer, Pat. DE19649880A1 (2 Dec. 1996).
[22] W. Pfeiffer, Pat. DE19638705A1 (21 Sept. 1996).
[23] N.A. Izmaiov, M.S. Shraiber, Farmazia 3 (1938) 1.
[24] K. Brendel, R.S. Steele, E.A. Davidson, J. Chromatogr. 30 (1967) 232.
[25] T. Gu, G.J. Tsai, G.T. Tsao, Chem. Eng. Sci. 46 (1991) 1279.
[26] T. Gu, G.J. Tsai, G.T. Tsao, Adv. Biochem. Eng. 469 (1993) 77.
[27] J. Baer, Dynamics of Fluids in Porous Media, Elsevier, New York, 1972, Ch. 5.3.2, p. 127.
[28] C.A. Zille, E.S. Della Monica, Arch. Biochem. Biophys. 58 (1955) 31.
[29] W.V. Epstein, M. Tan, J. Chromatogr. 6 (1961) 258.
[30] R.N. Sargenz, D.L. Graham, Anal. Chim. Acta 30 (1964) 101.
[31] T.P. King, Biochemistry 11 (1972) 367.
[32] J. Porath, Nature 196 (1963) 47.
[33] M. Lisso, W. Arlt, G. Wozny, Y.A. Beste, Pat. DE19900684A1 (4 Jan. 1999)
[34] M. Lisso, G. Wozny, W. Arlt, G. Mann, presented at the 8th International Symposium on Preparative and Industrial Chromatography and Allied Techniques, 2000.
[35] W. Pfeiffer, Pat. DE2970751.1 (3 July 1997).
[36] A. Daniov, L.G. Mustaeva, I.V. Vagenina, M.B. Baru, J. Chromatogr. A 732 (1996) 17.
[37] H. Determann, Gel Chromatography, 2nd ed., Springer, New York, 1969, p. 67.
[38] W. Heitz, Ber. Bunsen. Ges. 77 (1977) 210 (therein Ref. [8]: K. Ungerer, personal communication).
[39] I.V. Vagenina, E.A. Kozlovsky, L.G. Mustaeva, E.Y. Gorbunova, M.B. Baru, J. Chromatogr. A 840 (1999) 281.
[40] R.H. Perry, D.W. Green, J.M. Maloney, Perry's Chemical Engineer's Handbook, 7th ed, McGraw-Hill, New York, 1997.
[41] Application Brochure, Sephadex G-25, Amersham, Uppsala.
[42] J. Comiti, N.E. Sabiri, A. Montillet, Chem. Eng. Sci. 55 (2000) 3057.
[43] R.P. Chhabra, J. Comiti, I. Machai, Chem. Eng. Sci. 56 (2001) 1.
[44] B. Eisfeld, K. Schnitzlein, Chem. Eng. Sci. 56 (2001) 4321.
[45] R.K. Niven, Chem. Eng. Sci. 56 (2002) 527.
[46] M. Leva, Chem. Eng. 56 (1949) 115.
[47] M. Leva, Fluidization, McGraw-Hill, New York, 1959.
[48] T. Farkas, G. Zhong, G. Guichon, J. Chromatogr. A 849 (1999) 35.
[49] A. Felinger, G. Guichon, Biotechnol. Prog. 9 (1993) 450.
[50] G. Guiochon, M. Sarker, J. Chromatogr. A 704 (1995) 247.
[51] K. Ueyama, S. Furusaki, Chem. Eng. Comm. 36 (1985) 299.
[52] K.H. Parker, R.V. Mehta, C.G. Caro, J. Appl. Mech. (ASME) 54 (1987) 794.
[53] A.D. Mohammad, D.G. Stevenson, P.C. Wankat, Ind. Eng. Chem. Res. 31 (1992) 849.
[54] G.A. Soriano, N.J. Titchener-Hooker, P.A. Shamlou, Bioprocess Eng. 17 (1997) 115.
[55] K.C.E. Östergren, C. Trägardh, Numer. Heat Transf. A 32 (1997) 247.
[56] K.C.E. Östergren, C. Trägardh, G.G. Enstad, J. Mosby, AIChE J. 44 (1998) 2.
[57] K.C.E. Östergren, C. Trägardh, Chem. Eng. J. 72 (1999) 153.
[58] T. Lachab, C. Weill, Europ. Phys. J. B 9 (1999) 59.
[59] Q. Li, V. Rudolph, F. Wang, S. I. Kajikawa, M. Horio, http://www.postgrad.cheque.up.edü.au/research_groups/energy/2U.pdf
[60] A.G. Dixon, D.L. Cresswell, AIChE J. 25 (1979) 663.
[61] A. Brandt, G. Mann, W. Arlt, J. Chromatogr. A 769 (1997) 109.
[62] G. Mann, presented at PREP'90, Ghent.
[63] D. Johanson, personal communication on SPICA 2002, Heidelberg.
[64] W. Pfeiffer, W. Hörz, T. Igo-Kemenes, H.G. Zachau, Nature 258 (1975) 450.
[65] H.R. Maurer, Disc Electrophoresis, Walter de Gruyter, New York, 1971.
[66] K.J. Lissant, J. Colloid Interf. Sci. 22 (1966) 462.
[67] S.T. Eckersley, A. Rudin, J. Coating Techn. 780 (1990) 89.
[68] Y. Chevallier, C. Pichot, C. Graillat, M. Joanicot, K. Wong, J. Maquet, P. Lindner, B. Cabane, Coll. Polym. Sci. 270 (1992) 806.
[69] Y.C. Liao, D.J. Lee, P. He, Powder Technol. 123 (2002) 1.
[70] R.G. Carbonell, N.W. Han, J. Bhakta, AIChE J. 31 (1985) 277.
[71] D.C. Hong, P.V. Quinn, S. Luding, cond-mat/0010459 (2000).
[72] D.C. Hong, P.V. Quinn, S. Luding, Phys. Rev. Lett. 86 (2001) 3423.
[73] W. Pfeiffer, personal communication, 19 Aug. 1998.
[74] W. Pfeiffer, personal communication, 10 Oct. 1999.
[75] P.C. Carman, Trans. Inst. Chem. Eng. 15 (1937) 150.